Striving To Understand the Photophysics and Photochemistry of Thiophosgene: A Combined CASSCF and MR−CI Study

Ling Lin, Feng Zhang, Wan-Jian Ding, Wei-Hai Fang,* and Ruo-Zhuang Liu*

Department of Chemistry, Beijing Normal University, Beijing 100875, China

Received: September 5, 2004; In Final Form: November 8, 2004

The potential energy surfaces for Cl_2CS dissociation into ClCS + Cl in the five lowest electronic states have been determined with the combined complete active space self-consistent field (CASSCF) and MR−CI method. The wavelength-dependent photodissociation dynamics of Cl_2CS have been characterized through computed potential energy surfaces, surface crossing points, and CASSCF molecular dynamics calculations. Irradiation of the Cl_2CS molecules at 360−450 nm does not provide sufficient internal energy to overcome the barrier on S_1 dissociation, and the S_1/T_2 intersection region is energetically inaccessible at this wavelength region; therefore, $S_1 \rightarrow T_1$ intersystem crossing is the dominant process, which is the main reason S_1-S_0 fluorescence breaks off at excess energies of 3484−9284 cm^{-1}. Also, the $S_1 \rightarrow T_2$ intersystem crossing process can take place via the S_1-T_2 vibronic interaction in this range of excess energies, which is mainly responsible for the quantum beats observed in the S_1 emission. Both S_2 direct dissociation and $S_2 \rightarrow S_3$ internal conversion are responsible for the abrupt breakoff of S_2-S_0 fluorescence at higher excess energies. S_2 direct dissociation leads to the formation of the fragments of $Cl(\tilde{X}^2P)$ + $ClCS(\tilde{A}^2A'')$ in excited electronic states, while $S_2 \rightarrow S_3$ internal conversion followed by direct internal conversion to the ground electronic state results in the fragments produced in the ground state.

Introduction

Carbonyl compounds have been extensively studied over the past 20 years[1−5] because they play an important role in the development of our understanding of the spectroscopy, photochemistry, and photophysics of polyatomic molecules. Recent research suggests that thiocarbonyls may prove equally important in the future development of these areas. Thiocarbonyls and the parent carbonyls exhibit bonding properties that are qualitatively similar to one another. However, the lower electronic negativity of the sulfur atom and the higher polarization of the C═S bond lead to great differences in the photochemistry and photophysics of the two classes of compounds.[6] The photophysics, photochemistry, and related spectroscopy of thiocarbonyls have been reviewed by Maciejewski and Steer,[7] which follows three previous reviews concerning wavelength-dependent photochemistry,[8] the structure and excited-state dynamics of small thiocarbonyls,[9] and intramolecular relaxation processes of thiones in solution.[10]

As one of the simplest thiocarbonyls, thiophosgene (Cl_2CS) has been the subject of numerous experimental studies, which focus mainly on the photochemical and photophysical behavior of Cl_2CS. Thiophosgene absorbs weakly in the visible region to produce the lowest triplet (T_1) and lowest singlet (S_1) excited states, which correspond to a symmetry-forbidden $n \rightarrow \pi^*$ electron promotion.[6,7] The band origins of the $S_1 \leftarrow S_0$ and $T_1 \leftarrow S_0$ absorption systems were determined to be at 18 716 and 17 492 cm^{-1}, respectively, in the gas phase.[9] The C−S-stretching and out-of-plane-bending modes are active in the visible spectra of Cl_2CS, and the structures of the S_1 and T_1 states were determined by an analysis of these spectra. Measurement of the decay rates revealed that S_1-S_0 fluorescence begins to break off at an excitation of ~3500 cm^{-1} above the zero-point level of the S_1 state.[11] The abrupt breakoff of S_1-S_0 fluorescence is due to the S_1 dissociation of Cl_2CS into ClCS + Cl.[12] The absorption, emission, and excitation spectra of Cl_2CS in the S_1 and T_1 states have been measured in a perfluoroalkane solvent at room temperature.[13] The quantum yield of intersystem crossing (ISC) from S_1 to T_1 is estimated to be less than 0.4 in a perfluoroalkane solution, and the T_1 state decays almost exclusively by direct ISC to S_0. Recent studies that involve the S_1, T_1, and S_0 states of Cl_2CS focus mainly on radiationless transitions among the three electronic states. It was found that none of the $T_1 \leftarrow S_0$ bands in the cavity ringdown spectrum appear in the excitation spectrum,[14] indicating that the T_1 thiophosgene decays almost exclusively by nonradiative $T_1 \rightarrow S_0$ ISC. The T_1 nonradiative lifetime was estimated to be 20−50 ps. $S_1 \rightarrow S_0$ internal conversion (IC) was found to be inefficient for Cl_2CS in the gas phase,[15] which is most likely due to the absence of a promoting mode. Two-color optical−optical double-resonance studies[16] of the $T_1 \rightarrow S_0$ ISC process in jet-cooled thiophosgene indicate that rotational symmetry strongly influences the efficiency of ISC in symmetric molecules with low degrees of rotational excitation. Thiophosgene, thioformaldehyde, thiocyclobutanone, and thiocyclopentanone were found to exhibit very different emission characteristics,[17] and this difference was rationalized on the basis of the presence or absence of the promoting mode for $S_1 \rightarrow S_0$ IC and the extent of nonplanarity at the thiocarbonyl center. The collision-free S_1 thiophosgene does not exhibit radiationless transitions to bound electronic states at excess vibrational energies <3484 or >9284 cm^{-1}, which is evidenced by intense $S_1 \rightarrow S_0$ fluorescence with a nearly constant lifetime.[18] In the intermediate range of excess energies, fluorescence was not observed from the S_1 state of Cl_2CS, which is attributed to the occurrence of predissociation.

* Authors to whom correspondence should be sent. E-mail: Fangwh@bnu.edu.cn (W.-H.F.) and Rzliu@bnu.edu.cn (R.-Z.L.).

10.1021/jp046000t CCC: $30.25
Published on Web 01/06/2005

Over the past 3 decades, repeated attempts have been made to measure the S_2-S_0 absorption and emission spectra of thiophosgene vapor. The S_2-S_0 absorption spectrum consists of a complex system of discrete bands superimposed on and gradually merging into an underlying continuum at higher energies.[19] This band system was assigned to a spin-and-orbital-symmetry-allowed $\pi \rightarrow \pi^*$ transition. Excitation of Cl_2CS to low vibrational levels of the S_2 state results in strong fluorescence, but fluorescence weakening was observed at modest vibrational energies.[20−22] Two progressions in the S_2-S_0 absorption spectrum were identified by Judge and Moule,[23] and a weak band at 34 728 cm^{-1} was assigned as the origin. The three a_1 and one b_2 vibrations were determined for the S_2 state of Cl_2CS,[24] none of which corresponds to those observed by Judge and Moule. This controversy was settled in subsequent laser-induced fluorescence (LIF) spectrum studies.[25,26] The S_2-S_0 fluorescence excitation spectrum begins to break off at a vibrational energy of 1450 ± 50 cm^{-1} above the zero point of the S_2 state.

The ClCS and Cl_2 fragments were detected by the 248 nm laser photolysis of a pulsed molecular beam of thiophosgene.[27] These fragments, formed under collision-free conditions, were explained by two decomposition pathways

$$Cl_2CS + h\nu \rightarrow ClCS + Cl \quad \text{(a)}$$

$$\rightarrow Cl_2 + CS \quad \text{(b)}$$

The photodissociation dynamics of Cl_2CS at 235 nm have been studied by employing the resonance-enhanced multiphoton ionization and time-of-flight technique.[28] It was found that Cl atoms and ClCS radicals were formed in the ground and excited states. A particularly interesting photophysical property of S_2 thiophosgene was found to be the decrease in the intensity and shortening of the lifetime of S_2-S_0 fluorescence with increasing excess vibrational energies in the region below the threshold for dissociation.[29] The shortening of the lifetime and the loss of fluorescence at higher vibrational excitation energies were attributed to the crossing of the S_2 and S_3 electronic states.[30] A dark S_3 state was suggested to be in the vicinity of the S_2 state in an optical−optical double-resonance experiment.[31] A special xenon matrix detector has been used to study the production of $S(^1S)$ following controlled electron impact on thiophosgene targets over an electron energy range from the threshold to 400 eV.[32]

Although numerous experimental studies have been devoted to the electronic spectroscopy, photophysical, and photochemical processes of thiophosgene, the intramolecular dynamics of the excited states are largely unknown. As far as we know, there are only four reports[14,33−35] that involve ab initio calculations that concern the electronic states of Cl_2CS. The S_0 pathways for Cl_2CS decompositions into ClCS + Cl and CS + Cl_2 were investigated using Hartree−Fock (HF) calculations with small basis sets.[33,34] Because electron correlation is not included in the HF calculation, the reaction pathways traced by the HF method are only qualitatively reliable. The S_2 potential energy surface was constructed on the basis of complete active space self-consistent field (CASSCF) calculations, experimental vibrational frequencies, and tunneling splittings.[35] Complementary to the experimental work, Moule and co-workers[14] have carried out the MP2/6-31G(d,p) optimizations of the S_0 and T_1 equilibrium geometries of Cl_2CS. It is obvious that only limited theoretical information is available for the excited states of Cl_2CS.

Transitions to the S_2 state occur in the near-UV region, and the five lowest-lying electronic states (S_0, S_1, S_2, T_1, and T_2) must be considered when describing the photochemistry and photophysics of thiophosgene. This is one of the reasons why theoretical investigations of the photodissociation dynamics of Cl_2CS are not yet up to date. In the present work, we have carried out a combined CASSCF and MR−CI study on the S_0, S_1, S_2, T_1, and T_2 potential energy surfaces for Cl_2CS dissociations to ClCS and Cl. The intersection structures of these electronic states were characterized with state-averaged CASSCF calculations. Ab initio molecular dynamics calculations at the CASSCF level have been performed to explore the initial relaxation dynamics after photoexcitation. We believe that the results reported here provide new insights into the photochemical and photophysical processes of thiophosgene and related thiocarbonyls.

Computational Methods

The stationary structures on the S_0, S_1, S_2, T_1, and T_2 surfaces have been fully optimized with the CASSCF method. For comparison, the MP2 method has also been used to determine the S_0 and T_1 stationary structures. The nature of critical points (equilibrium geometries and transition states) is confirmed to be a minimum or first-order saddle point by frequency computations. The state-averaged CASSCF method has been used to determine the geometry of the intersection space. The 6-311G* and cc-pVTZ basis sets are employed in the present work to optimize structures and to calculate energies. All ab initio calculations have been performed using the GAUSSIAN 03 and MOLPRO packages of programs.[36,37]

The selection of the active space is a crucial step for the CASSCF calculations. The preliminary CASSCF calculations were performed with a small active space that comprises eight electrons in seven orbitals, referred to as CAS(8,7). The eight active electrons originate from the C=S π orbital, the nonbonding orbital of the S atom, and the $3p_z$ orbitals of two Cl atoms. The CAS(8,7) calculations give a good description of the equilibrium structures and relative energies of the S_0, T_1, and S_1 states. For a balanced description of the C−Cl dissociation process, the two C−Cl σ orbitals should be added to the active space. Thus, all of the stationary structures are optimized at the CASSCF level with 12 electrons in 10 orbitals. Besides the six occupied orbitals, the C−S π^*, C−Cl, and C−S σ^* orbitals are used as the active orbitals. It should be pointed out that the three σ^* orbitals in the active space are actually delocalized into the whole molecular backbone, with remarkable antibonding characteristics in the C−Cl or C−S region.

To refine the relative energies of the stationary structures, the single-point energy is calculated with an internally contracted MR−CI method that includes all single and double excitations relative to the CASSCF reference wave functions. A total of 24 valence electrons and all of the virtual orbitals are included in the MR−CI/cc-pVTZ correlation calculations. The MOLPRO program package[37] was used to perform the MR−CI single-point energy calculations.

Molecular dynamics calculations on the CASSCF potential energy surface have been performed with the second-order Hessian-based integration method developed by Helgaker and co-workers.[38] A local quadratic surface can be constructed from the analytic first and second derivatives of the energies calculated by using the CASSCF method:

$$V(x) = E^\circ + G^{\circ t}(x - x^\circ) + \frac{1}{2}(x - x^\circ)^t H^\circ (x - x^\circ) \quad (1)$$

where E°, G°, and H° are the energy, gradient, and Hessian

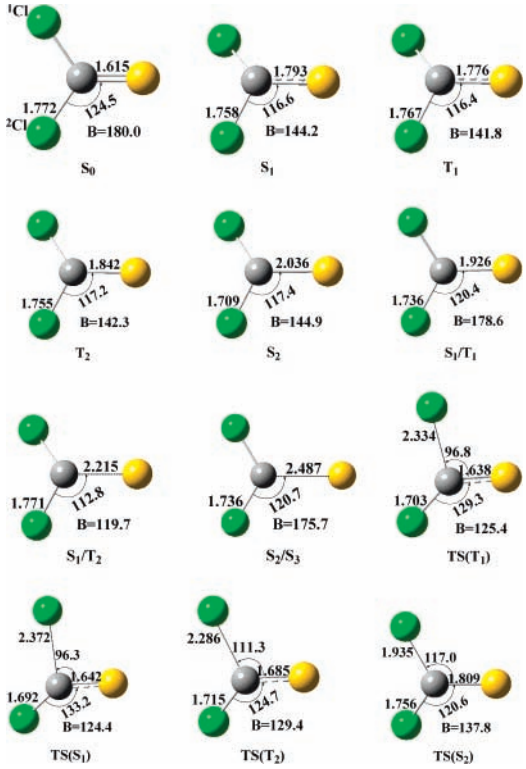

Figure 1. Schematic structures of the stationary and intersection points on the S_0, S_1, S_2, T_1, and T_2 surfaces of Cl_2CS, along with the selected CAS(12,10)/6-311G* bond parameters (bond lengths in Å, bond angles in deg, and B = the Cl−C−S−Cl dihedral angle).

evaluated at $x°$, respectively. In Cartesian coordinates, the classic equations of motion on the quadratic surface are given by

$$m_i \frac{d^2 x_i}{dt^2} = -\frac{dV(x)}{dx_i} = -G_i° - \sum_j H_{ij}°(x - x_j°) \qquad (2)$$

The local second-order surface is a good approximation of the true surface only in a small region around the expansion point, and the calculated trajectory is not allowed to leave this region. An improved method[39] using the fifth-order polynomial fitted surface was used in the present molecular dynamics calculations.

Results and Discussion

S_0, S_1, S_2, T_1, and T_2 Equilibrium Structures. Equilibrium structures of the S_0, S_1, S_2, T_1, and T_2 states are shown in Figure 1 along with the key bond parameters optimized at the CAS-(12,10)/6-311G* level. The experimentally inferred S_0 structure of Cl_2CS[7] is reproduced using the MP2/cc-pVTZ calculation. In comparison, the C−Cl bond length is a little overestimated by the CAS(12,10)/6-311G* computations. Cl_2CS is planar with C_{2v} symmetry in its ground state, which is well-known.[7] When excited to S_1 from S_0, the four atoms are no longer coplanar and the symmetry is reduced to C_s from C_{2v}. The out-of-plane angle is predicted to be 35.8° by the CAS(12,10)/6-311G* calculations, which is close to the 32° inferred experimentally.[7] The second striking feature of the S_1 structure is a significant increase of the C−S bond length, which is 1.615 Å in S_0 and becomes 1.793 Å in S_1 at the CAS(12,10)/6-311G* level. The S_1 structural features coincide with the fact that the S_1 state originates from the $n \rightarrow \pi^*$ transition. Also arising from the $n \rightarrow \pi^*$ electron promotion, the T_1 state is similar to the S_1 state in structure. However, the C−S bond length is shorter and the C−Cl bond length is longer in the T_1 structure with respect to those in the S_1 structure.

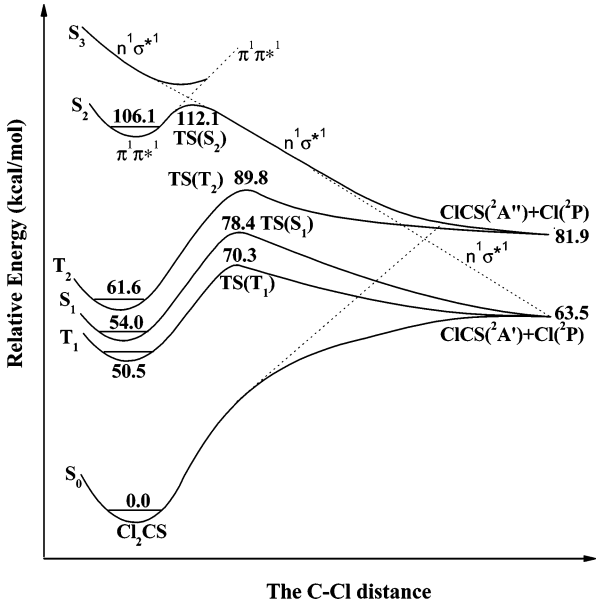

Figure 2. Adiabatic potential energy profiles for the Cl_2CS dissociations into ClCS + Cl in the five lowest electronic states, together with the MR−CI/cc-pVTZ relative energies (kcal/mol) for the equilibrium and transition state structures. The relative energies of the fragments come from previous experiments and calculations (refs 7 and 12). Some diabatic state correlations for the dissociations are plotted in dotted lines, with the main $n^1\sigma^{*1}$ or $\pi^1\pi^{*1}$ electronic configuration.

The S_2 equilibrium structure was predicted to be nonplanar with an out-of-plane angle of 35.1° and a C−S bond length of 2.036 Å. The out-of-plane angle and the C−S bond length of the S_2 state were experimentally inferred to be about 30° and 2.1 Å, respectively.[23−25] The C−S bond length in S_2 is much longer than the corresponding values of 1.793 Å in S_1 and 1.615 Å in S_0, which is consistent with a nominal decrease in the C−S bond order from 2.0 to 1.5 and to 1.0 upon $n \rightarrow \pi^*$ and $\pi \rightarrow \pi^*$ excitations. The T_2 state is confirmed to be of $^3\pi\pi^*$ character by the CAS(12,10)/6-311G* calculations, but its equilibrium C−S bond length of 1.842 Å is much shorter than that in the S_2 equilibrium structure. Relative to the T_2 state, the stronger correlation of the two π electrons in S_2 is responsible for significantly lengthening the C−S bond in the S_2 structure.

The third excited singlet state (S_3) plays an important role in the photodissociation dynamics of Cl_2CS. We attempted to optimize the equilibrium geometry of the S_3 state at the CAS-(12,10)/6-311G* level but were unsuccessful. The S_3 potential energy profile for the C−Cl bond cleavage was scanned using the MR−CI stepwise calculations, with all other bond parameters kept at the ground-state equilibrium values. The MR−CI calculations show that the S_3 state is of the $^1n\sigma^*$ character in the Franck−Condon (FC) region. As shown in Figure 2, the $n^1\sigma^{*1}$ configuration makes a main contribution to the S_2 wave function in the C−Cl distance range of 2.0−3.0 Å. Furthermore, the S_0 wave function is dominated by the $n^1\sigma^{*1}$ configuration at a C−Cl distance longer than 3.0 Å. Actually, the S_3 state correlates diabatically with the fragments in the ground state.

Adiabatic Excitation Energies and Inversion Barriers. The calculated energies for the stationary and intersection points on the S_0, S_1, S_2, T_1, and T_2 surfaces are given in the Supporting Information. The adiabatic excitation energies from S_0 to T_1, S_1, T_2, and S_2 were predicted to be 51.9, 54.4, 63.2, and 113.4 kcal/mol by the CAS(12,10)/6-311G* calculations, respectively. They become 50.5, 54.0, 61.6, and 106.1 kcal/mol, respectively,

using the MR−CI/cc-pVTZ single-point energy calculations on the CAS(12,10)/6-311G* optimized structures. The T_1 and S_1 origins were assigned at 17 492 cm^{-1} (50.0 kcal/mol) and 18 716 cm^{-1} (53.5 kcal/mol) on the basis of an analysis of vibrational structures in the absorption spectrum.[24] On the basis of the threshold energy for the observation of beat-modulated fluorescence decay from the S_1 state, the T_2 origin was placed at about 20 340 cm^{-1} (58.2 kcal/mol).[18] The S_2 origin was experimentally inferred to be in the range of 33 991−36 010 cm^{-1} (97.2−103.0 kcal/mol).[23−25] In comparison with the S_1, S_2, T_1, and T_2 band origins, the combined CAS(12,11)/6-311G* and MR−CI/cc-pVTZ calculations provide a good description of the adiabatic excitation energies from the ground state to the four lowest excited states.

The S_2 structure with C_{2v} symmetry was optimized and confirmed to be the first-order saddle point that connects two equivalent minima on the S_2 surface. Analogous situations occur for the S_1, T_1, and T_2 states. This is consistent with the existence of a barrier to molecular inversion on the S_1, S_2, T_1, or T_2 state.[7,23−25] The barrier to molecular inversion on the S_2 surface was calculated to be 1383 cm^{-1} at the MR−CI level. The barrier was inferred to be 729 cm^{-1} for the S_2 states in early experiments[7,23−25] and was revised upward to 1495 cm^{-1} from an analysis of the inversion splitting extracted from the band intervals in one-photon LIF spectra.[30] The barrier heights were experimentally estimated to be in the range of 600−800 cm^{-1} for the molecular inversion on the S_1 and T_1 surfaces,[7,14] and these are close to the values calculated in the present work.

Dissociation of Cl_2CS into ClCS and Cl. The C−Cl bond cleavages along the S_0, S_1, S_2, S_3, T_1, and T_2 pathways were scanned using the MR−CI stepwise calculations, with all other bond parameters kept at the ground-state equilibrium values. On the basis of the MR−CI stepwise calculations, the state correlation diagram is determined for the dissociation processes. The Cl_2CS molecules in $S_2(^1\pi\pi^*)$ correlate adiabatically with the fragments of $Cl(\tilde{X}^2P)$ and $ClCS(\tilde{A}^2A'')$, which correspond to the first excited electronic state of the fragments. A transition state was found on the S_2 pathway and is referred to as $TS(S_2)$ hereafter. The C−^{1}Cl bond is 1.935 Å in the $TS(S_2)$ structure, which is a little longer than that in the S_2 equilibrium geometry. Because S_2 dissociation to $Cl(\tilde{X}^2P) + ClCS(\tilde{A}^2A'')$ is exothermic by 24.2 kcal/mol, the dissociation reaction has a $TS(S_2)$ geometry close to that of the S_2 reactant.[40] The barrier to the C−^{1}Cl bond cleavage along the S_2 pathway was calculated to be 6.3 and 6.0 kcal/mol at the CAS(12,10)/6-311G* and MR−CI/cc-pVTZ levels of theory, respectively. The potential energy surfaces for the dissociations are depicted in Figure 2 along with the MR−CI relative energies of the stationary structures.

The S_2-S_0 fluorescence excitation spectrum begins to break off at a vibrational energy of 1450 ± 50 cm^{-1} above the zero point of the S_2 state and was attributed to C−Cl bond dissociation.[25,26] Under free jet expansion, the loss of S_2-S_0 fluorescence was found to occur at about 1700 cm^{-1} above the electronic origin of the S_2 state.[18,31] These experimental results reveal that the barrier height is in the range of 4−5 kcal/mol for the C−Cl bond fission along the S_2 pathway, which is very close to the 6.0 kcal/mol predicted by the present calculations. The quantum yield of Cl production from Cl_2CS was observed to be unity and pressure independent at excitation wavelengths shorter than 253.7 nm, which indicates that Cl_2CS dissociation to ClCS + Cl is the only primary process and the dissociation must be direct.[12] Recently, photodissociation dynamics of Cl_2CS at 235 nm have been investigated employing the resonance-enhanced multiphoton ionization and time-of-flight technique.[28] It was found that the ClCS fragments are produced in the ground and excited states.

The Cl_2CS molecules in $S_1(^1n\pi^*)$ correlate adiabatically with the fragments of $Cl(\tilde{X}^2P)$ and $ClCS(\tilde{X}^2A')$ in the ground state. A transition state was found on the S_1 pathway and is referred to as $TS(S_1)$ hereafter. The C−^{1}Cl bond is nearly broken in $TS(S_1)$ with a C−^{1}Cl distance of 2.372 Å, which is much longer than that in $TS(S_2)$. The MR−CI calculations show that the S_1 dissociation of Cl_2CS to $Cl(\tilde{X}^2P) + ClCS(\tilde{X}^2A')$ is endothermic by 9.5 kcal/mol. The long C−^{1}Cl distance in $TS(S_1)$ is consistent with Hammond's postulate:[40] the endothermic reaction has a transition-state geometry close to that of the product. The barrier to the C−^{1}Cl bond cleavage along the S_1 pathway was predicted to be 24.4 kcal/mol by the MR−CI/cc-pVTZ calculations on the CAS(12,10)/6-311G* structures.

Two transition states were found on the T_1 and T_2 dissociation pathways and are referred to as $TS(T_1)$ and $TS(T_2)$, respectively. As shown in Figure 1, the $TS(T_1)$ and $TS(T_2)$ structures are similar to the $TS(S_1)$ geometry with a C−^{1}Cl distance of about 2.3 Å. The T_1 dissociation reaction has a barrier of 19.8 kcal/mol at the MR−CI/cc-pVTZ level, which is a little lower than that on the S_1 pathway. However, the barrier height is 28.2 kcal/mol for T_2 dissociation, which is a little higher than that on the S_1 pathway. The T_2 dissociation of Cl_2CS correlates adiabatically with the fragments of $Cl(\tilde{X}^2P)$ and $ClCS(\tilde{A}^2A'')$ in the excited electronic state and has high endothermic character, which is one of the reasons that a high barrier exists on the T_2 pathway. We have tried our best to locate a transition state for the C−Cl bond cleavage in the ground state, but optimizations always lead to the dissociation limit of $Cl(\tilde{X}^2P)$ and $ClCS(\tilde{X}^2A')$. C−Cl dissociation is endothermic by 63.5 kcal/mol in the ground state, and no barrier exists on the S_0 pathway.

Radiationless Transitions. Electronic radiationless transitions in the Cl_2CS molecules have been extensively investigated,[14−17] mainly on the basis of the rate theory of radiationless transition developed by Lin.[41] A transition from one electronic state to another of lower energy is subject to symmetry selection. The planar C_{2v} point group is appropriate for describing radiationless transitions in the Cl_2CS molecule. IC between the $S_2(^1A_1)$ and $S_1(^1A_2)$ states requires a promoting mode of a_2 vibrational symmetry to render the vibronic coupling matrix elements of the two states finite.[14−17] The same situation occurs for the $S_1(^1A_2) \rightarrow S_0(^1A_1)$ IC process. However, the present frequency calculations and the previous experimental study[17] reveal that thiophosgene lacks the promoting mode of a_2 symmetry. Thus, the $S_2 \rightarrow S_1$ and $S_1 \rightarrow S_0$ IC processes are very inefficient for Cl_2CS.

A minimum-energy crossing point (S_3/S_2) between the S_3 and S_2 surfaces was found using state-averaged CAS(12,10)/6-311G* calculations. The S_3/S_2 intersection has a quasi-planar C_{2v} structure with a C−S distance of 2.487 Å at the CAS(12,-10)/6-311G* level, which is close to that predicted by the CAS-(6,6) calculations.[35] However, the C−Cl distance was fixed at 1.68 Å in that study,[35] which is quite different from the 1.736 Å optimized in the present study. The S_3/S_2 intersection is about 4 kcal/mol higher than the $TS(S_2)$ transition state in energy. The abrupt breakoff of S_2-S_0 fluorescence at higher excess energies has been attributed to the crossing of the S_3 and S_2 electronic states at long C−S distance in recent studies.[29−31,35]

To explore the probability of ISC between the singlet and triplet states, the intersection structures among the S_2, T_1, and T_2 states were optimized with the state-averaged CAS(12,10)/6-311G* methods. It was found that the S_2/T_1 and S_2/T_2 intersection structures are close to the dissociation limit of Cl_2C-

($\tilde{X}^1A_1$) + S(^3P) with relatively high energies. It is obvious that the two intersection structures are not responsible for the $S_2 \rightarrow T_1$ and $S_2 \rightarrow T_2$ ISCs. The relatively large electronic energy gap (55.6 kcal/mol) between the $S_2(^1\pi\pi^*)$ and $T_1(^3n\pi^*)$ states leads to a strong FC inhibition of the rates of the $S_2 \rightarrow T_1$ radiationless decay. In addition, ISC from S_2 to T_1 is a spin-forbidden process, although the spin−orbit interaction of the two states is strong. It is reasonable to expect that the $S_2 \rightarrow T_1$ ISC process takes place with little probability. There is a lesser probability for $S_2 \rightarrow T_2$ ISC because no first-order spin−orbit interaction exists between the $S_2(^1\pi\pi^*)$ and $T_2(^3\pi\pi^*)$ states. Inefficiency of a radiationless transition from S_2 to T_1 or T_2 is consistent with the strong S_2-S_0 fluorescence at low excess energies.[22−25]

The energy differences among the S_1, T_1, and T_2 minima are very small, and the three states probably intersect in the FC region. A crossing point (S_1/T_1) between the S_1 and T_1 surfaces was found using state-averaged CAS(12,10)/6-311G* calculations. As shown in Figure 1, the S_1/T_1 structure is nearly planar, with a Cl−C−S−Cl dihedral angle of 178.6°. In comparison to the S_1 equilibrium structure, the C−S bond is elongated by 0.133 Å and the C−Cl bond is shortened by 0.022 Å in the S_1/T_1 structure. Actually, the S_1/T_1 intersection is similar to the planar S_1 saddle point in structure, except for the C−S bond that is a little longer in S_1/T_1. With respect to the S_1 minimum, the S_1/T_1 intersection has an energy of 5.4 kcal/mol at the CAS-(12,10)/6-311G* level. The spin−orbit coupling matrix element at the S_1/T_1 structure was calculated to be 2.8 cm^{-1} by using MR−CI wave functions and full Breit−Pauli spin−orbit coupling operators. Both the S_1 and T_1 states originate from $n \rightarrow \pi^*$ electron promotion, and they have the same electronic configuration. Therefore, there is no first-order spin−orbit interaction[42] between the two states. This provides a reasonable explanation for why the spin−orbit coupling matrix element is very small at the S_1/T_1 intersection structure.

The minimum-energy crossing point (S_1/T_2) between the S_1 and T_2 surfaces was determined using state-averaged CAS-(12,10)/6-311G* calculations. The S_1/T_2 structure has a C_s symmetry with an out-of-plane angle of 60.3° and C−Cl and C−S bond lengths of 1.771 and 2.215 Å, respectively. The significant changes in the S_1/T_2 structure, compared to the S_1 equilibrium geometry, are associated with the out-of-plane angle and C−S bond length. Relative to the S_1 minimum, the S_1/T_2 intersection has an energy of 24.7 kcal/mol at the CAS(12,10)/6-311G* level. The S_1/T_2 crossing point is much higher than the S_1/T_1 intersection in energy. The spin−orbit coupling matrix element at the S_1/T_2 structure was calculated to be 131.6 cm^{-1} by using MR−CI wave functions and full Breit−Pauli spin−orbit coupling operators, and this value is much larger than that at the S_1/T_1 intersection. Because the S_1 state is of the $^1n\pi^*$ character and the T_2 state arises from $\pi \rightarrow \pi^*$ electron transition, the spin−orbit interaction between the S_1 and T_2 states is strong.[42] This is consistent with a larger spin−orbit coupling matrix element in the S_1/T_2 structure.

Dynamics of the S_2 State. Irradiation of Cl_2CS at 253 nm or shorter wavelengths results in the Cl_2CS molecules being populated in the S_2 state. There are five radiationless routes for the S_2 molecules to deactivate: the $S_2 \rightarrow S_1$ and $S_2 \rightarrow S_3$ radiationless decays, the $S_2 \rightarrow T_1$ and $S_2 \rightarrow T_2$ ISC processes, and the S_2 dissociation to Cl($\tilde{X}^2P$) + ClCS($\tilde{A}^2A''$). As pointed out before, $S_2 \rightarrow S_1$ IC is very inefficient because of the absence of the promoting mode of a_2 vibrational symmetry. The S_2/T_1 and S_2/T_2 intersection structures are close to the dissociation limit of $Cl_2C(\tilde{X}^1A_1)$ + S(^3P) with relatively high energies, which are not responsible for $S_2 \rightarrow T_1$ and $S_2 \rightarrow T_2$ ISCs. The vibronic interaction between the S_2 and T_1 states is weak because of the relatively large electronic energy gap that leads to a strong FC inhibition of the rates of $S_2 \rightarrow T_1$ ISC. An analogous situation was expected to occur for the $S_2 \rightarrow T_2$ ISC process. Thus, the $S_2 \rightarrow T_1$ and $S_2 \rightarrow T_2$ radiationless decays take place with little probability.

A particularly interesting photophysical property of S_2 thiophosgene is the decrease in intensity and shortening of the lifetime of S_2-S_0 fluorescence that occur with increasing excess energy in the region below the threshold (~1300 cm^{-1}). This was attributed to the crossing of the S_3 and S_2 electronic states at long C−S distance in several experimental studies.[29−31] The large C−S bond length in the S_3 state leads to very favorable FC factors for $S_3 \rightarrow S_0$ IC.[30,31] If $S_2 \rightarrow S_3$ IC followed by direct IC to the ground electronic state is the only route for S_2 deactivation at excess energies larger than 1700 cm^{-1}, the fragments are formed only in the ground state. However, it was found that the ClCS radicals are mainly produced in the excited electronic state upon photoexcitation of Cl_2CS at 235 nm.[28]

The loss of S_2-S_0 fluorescence at higher excess energies was attributed to the S_3/S_2 intersection, which is, to a large extent, based on the CAS(6,6) calculations of Strickler and Gruebele.[35] However, the S_2 potential energy surface as a function of the C−S distance and the out-of-plane angle was fitted with the C−Cl bond lengths and Cl−C−S bond angles fixed at the S_2 equilibrium values, and there is no information available for the C−Cl bond cleavage along the S_2 pathway.[35] The present calculations indicate that S_2 dissociation to Cl($\tilde{X}^2P$) + ClCS-($\tilde{A}^2A''$) is another important route for S_2 deactivation. In addition, the dominant ClCS fragment observed in the $\tilde{A}^2A''$ excited state[28] indicates that S_2 C−Cl bond cleavage has some preference over $S_2 \rightarrow S_3$ IC. This is consistent with the calculated result that TS(S_2) has lower energy relative to the S_3/S_2 intersection. It can be concluded from the present calculation that both S_2 dissociation to Cl($\tilde{X}^2P$) + ClCS($\tilde{A}^2A''$) and $S_2 \rightarrow S_3$ IC followed by direct IC to the ground state are responsible for the loss of S_2-S_0 fluorescence at higher excess energies.

Dynamics of the S_1 State. Similar to the S_2 state, there are four radiationless routes for the S_1 molecules to deactivate: $S_1 \rightarrow S_0$ radiationless decay, the $S_1 \rightarrow T_1$ and $S_1 \rightarrow T_2$ ISC processes, and S_1 direct dissociation to Cl($\tilde{X}^2P$) + ClCS($\tilde{X}^2A'$). As pointed out before, $S_1 \rightarrow S_0$ IC is very inefficient because of the absence of a promoting mode of a_2 vibrational symmetry. S_1 direct dissociation to Cl($\tilde{X}^2P$) + ClCS($\tilde{X}^2A'$) is an adiabatic process, and the TS(S_1) transition state is almost equal to the S_1/T_2 intersection in energy. Considering that the spin−orbit interaction is strong at the S_1/T_2 structure, $S_1 \rightarrow T_2$ ISC via the S_1/T_2 intersection may compete with S_1 direct dissociation. However, much energy is required to overcome the barrier on the S_1 direct dissociation pathway or to reach the S_1/T_2 intersection region. The two processes are not in competition with $S_1 \rightarrow T_1$ ISC via the S_1/T_1 intersection, which will be discussed below.

The S_1/T_1 structure is similar to the S_1 equilibrium geometry, while a large difference exists between the S_1 and S_1/T_2 structures. With respect to the S_1 minimum, the S_1/T_1 intersection has a relative energy of 5.4 kcal/mol, but the S_1/T_2 and TS(S_1) structures are respectively 25.7 and 24.4 kcal/mol above the S_1 origin. In view of the TS(S_1), S_1/T_1, and S_1/T_2 energies, $S_1 \rightarrow T_1$ ISC takes place much more easily than $S_1 \rightarrow T_2$ ISC and S_1 direct dissociation in the excess energy range of 10−30 kcal/mol. It should be pointed out that $S_1 \rightarrow T_1$ ISC is a spin-

forbidden process and the spin−orbit interaction is weak at the S_1/T_1 structure. On the basis of the calculated spin−orbit coupling matrix element (2.8 cm^{-1}) and differences of energy gradients at the S_1/T_1 intersection, the probability factor (a transition probability per passage through the crossing seam) from S_1 to T_1 is estimated to be 1.5×10^{-4} by the Landau−Zener law[43] with the excess energy at 3500 cm^{-1}. If $S_1 \rightarrow T_1$ ISC is treated as a spin-allowed process, the rate coefficient is calculated to be 2.4×10^{11} s^{-1} using the RRKM rate theory of unimolecular reaction. The spin-forbidden $S_1 \rightarrow T_1$ ISC process should have a rate coefficient of $\sim 3.6 \times 10^{7}$ s^{-1} with the excess energy at 3500 cm^{-1}.

The T_2 state is only 7.6 kcal/mol above the S_1 zero-point level, and the S_1 and T_2 states have similar equilibrium structures. The vibronic interaction between the S_1 and T_2 states is strong near the T_2 equilibrium geometry because of the relatively small electronic energy gap and the relatively strong spin−orbit interaction that lead to a favorable FC factor and considerable hopping probability for $S_1 \rightarrow T_2$ ISC. $S_1 \rightarrow T_2$ ISC via the vibronic interaction is in competition with $S_1 \rightarrow T_1$ ISC through the S_1/T_1 intersection. As pointed out before, T_2 dissociation of Cl_2CS produces the fragments of $Cl(\tilde{X}^2P)$ + $ClCS(\tilde{A}^2A'')$ in an excited electronic state with a barrier of 28.2 kcal/mol. After the $S_1 \rightarrow T_2$ decay, T_2 dissociation takes place with little probability because of the high barrier on the pathway. Therefore, $S_1 \rightarrow T_2$ ISC via the vibronic interaction can have considerable influence on the S_1-S_0 fluorescence decays but does not play an important role in the S_1 dissociation processes.

To explore the initial relaxation processes from the S_1 FC geometry, molecular dynamics calculations have been performed on the local second-order approximation to the true surface with the fifth-order polynomial fits.[38,39] The initial conditions for trajectory calculations have been chosen to simulate the experimental photodissociation[18] of Cl_2CS at 28 000 cm^{-1}. The trajectory at 0 K is started from the S_1 FC geometry with a step size of 0.25 $amu^{1/2}$ bohr. The Cl−C−S−Cl dihedral angle and the C−S and C−Cl distances as a function of time are plotted in Figure 3. As pointed out before, the S_1/T_1 structure is nearly planar with a C−S bond length of 1.926 Å and a Cl−C−S−Cl dihedral angle of 178.6°. It can be seen from Figure 3 that the trajectory starts from FC geometry and reaches the S_1/T_1 intersection region many times within 2000 fs. However, the C−Cl distance is 2.372 Å in $TS(S_1)$, and the C−S distance is 2.215 Å in S_1/T_2; the trajectory is not propagated to the $TS(S_1)$ and S_1/T_2 structures within the same period. Molecular dynamics calculations clearly show that S_1 direct dissociation and $S_1 \rightarrow T_2$ ISC through the S_1/T_2 structure take place with little probability and $S_1 \rightarrow T_1$ ISC via the S_1/T_1 intersection region is an important route for S_1 deactivation.

After relaxation to the T_1 state, the Cl_2CS molecules either dissociate into $Cl(\tilde{X}^2P)$ + $ClCS(\tilde{X}^2A')$ along the T_1 pathway or decay to the ground state through $T_1 \rightarrow S_0$ ISC. T_1 direct dissociation has a barrier of 70.3 kcal/mol with respect to the S_0 zero-point level, which is energetically inaccessible upon photoexcitation of Cl_2CS at 435.8 nm (65.5 kcal/mol). However, the quantum yield of $Cl(\tilde{X}^2P)$ production was observed to be about 0.5 at this wavelength.[12] These show that the dissociation reaction may proceed along the S_0 pathway as a result of $T_1 \rightarrow S_0$ ISC. The rate theory of radiationless transition[41] was used to estimate the T_1 nonradiative lifetime,[14] which is based on the MP2 equilibrium structures and vibrational frequencies for the T_1 and S_0 states. The large matrix element of the T_1-S_0 spin−orbit coupling (150 cm^{-1}) and the favorable FC factors for $T_1 \rightarrow S_0$ ISC are responsible for the short T_1 nonradiative lifetime of ~20 ps.[14] Experimentally, it was found that none of the $T_1 \leftarrow S_0$ bands in the cavity ringdown spectrum appear in the excitation spectrum,[14] indicating that the T_1 thiophosgene decays almost exclusively by nonradiative $T_1 \rightarrow S_0$ ISC.

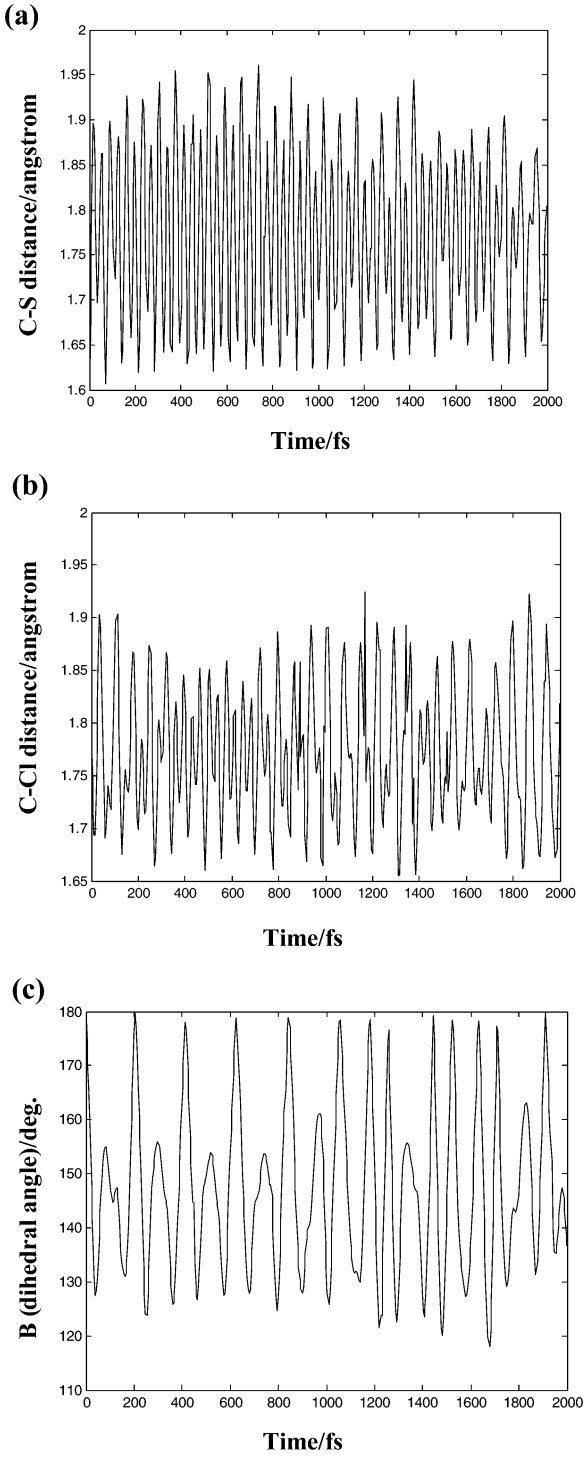

Figure 3. Plot of the selected bond parameters as a function of time: (a) C−S distance, (b) C−Cl distance, and (c) the Cl−C−S−Cl dihedral angle.

The $S_1 \rightarrow T_1$ and $S_1 \rightarrow T_2$ ISC processes take place with little probability at S_1 excess energies smaller than 6 kcal/mol, which is consistent with the experimental observation that S_1-S_0 fluorescence has a nearly constant lifetime at low excess energies.[18] At excess vibrational energies larger than 10 kcal/mol, the dissociation to $Cl(\tilde{X}^2P)$ + $ClCS(\tilde{X}^2A')$ occurs at a considerable rate, as a result of $S_1 \rightarrow T_1$ ISC followed by $T_1 \rightarrow S_0$ ISC. Measurement of the decay rates revealed that S_1-S_0

fluorescence begins to break off at an excitation of ~3500 cm^{-1} above the zero-point level of the S_1 state.[11,18] The abrupt breakoff of S_1-S_0 fluorescence was attributed to the dissociation of Cl_2CS into ClCS + Cl.[12,18] Also, the $S_1 \rightarrow T_2$ ISC process can take place via the S_1-T_2 vibronic interaction at large excess energies. Thiophosgene exhibits quantum beats in emission when it is excited to S_1 vibronic levels.[18] The reason for this probably comes from the S_1-T_2 vibronic interaction.

Summary

The potential energy surfaces for Cl_2CS dissociation into ClCS + Cl in the five lowest electronic states have been determined with the combined CASSCF and MR−CI method. The wavelength-dependent photodissociation dynamics of Cl_2CS have been characterized through computed potential energy surfaces, surface crossing points, and molecular dynamics calculations. When the S_1 excess energies are smaller than 3500 cm^{-1}, all of the radiationlesss processes from the S_1 state take place with little probability and the S_1 radiation decays occur with high quantum yield. Irradiation of the Cl_2CS molecules at 360−450 nm does not provide sufficient internal energy to overcome the barrier on S_1 dissociation, and the S_1/T_2 intersection region is energetically inaccessible at this wavelength region. In this case, $S_1 \rightarrow T_1$ ISC becomes a dominant process, which is followed by $T_1 \rightarrow S_0$ ISC and C−Cl bond cleavage in the ground state. This is the main reason S_1-S_0 fluorescence breaks off with excess energies of 3484−9284 cm^{-1}.[18] Also, the $S_1 \rightarrow T_2$ ISC process can take place via the S_1-T_2 vibronic interaction in this range of excess energies, which is mainly responsible for the quantum beats observed in the S_1 emission.

The loss of S_2-S_0 fluorescence at higher excess energies was only attributed to the S_3/S_2 intersection in the previous studies. Photodissociation of Cl_2CS into ClCS + Cl has been observed in many experiments in the wavelength range of 235−253 nm, but the role that dissociation plays in the S_2 dynamics of Cl_2CS has not been completely understood before. The present calculations indicate that S_2 dissociation to $Cl(\tilde{X}^2P)$ + ClCS($\tilde{A}^2A''$) has a barrier of 6.0 kcal/mol, and dissociation is an important route that is responsible for the abrupt breakoff of S_2-S_0 fluorescence at higher excess energies. S_2 direct dissociation leads to formation of the fragments of $Cl(\tilde{X}^2P)$ + ClCS($\tilde{A}^2A''$) in excited electronic states, while $S_2 \rightarrow S_3$ IC followed by direct IC to the ground electronic state results in the fragments produced in the ground state.

Acknowledgment. This work is supported by the National Natural Science Foundation of China (Grant 20233020) and the Major State Basic Research Development Programs (Grants 2004CB719903 and 2002CB613406).

Supporting Information Available: Structures and energies of the stationary and intersection points reported in the present work. This material is available free of charge via the Internet at http://pubs.acs.org.

References and Notes

(1) Wagner, P. J. In *CRC Handbook of Organic Photochemistry and Photobiology*; Horspool, W. M., Song, P.-S., Eds.; CRC Press: Boca Raton, FL, 1995; p 449.

(2) Diau, E. W.-G.; Kotting, C.; Zewail, A. H. *ChemPhysChem* **2001**, *2*, 273−293; **2001**, *2*, 294−309; **2001**, *3*, 57−78; **2001**, *3*, 79−97 and references therein.

(3) Griesbeck, A. G.; Heckroth, H. *J. Am. Chem. Soc.* **2002**, *124*, 396−403 and references therein.

(4) Fang, W.-H. *J. Am. Chem. Soc.* **1999**, *121*, 8376−8384. Fang, W.-H.; Liu, R.-Z. *J. Am. Chem. Soc.* **2000**, *122*, 10886−10894. Chen, X.-B.; Fang, W.-H.; Fang, D.-C. *J. Am. Chem. Soc.* **2003**, *125*, 9689−9698. He, H.-Y.; Fang, W.-H. *J. Am. Chem. Soc.* **2003**, *125*, 16139−16147 and references therein.

(5) Yamamoto, N.; Olivucci, M.; Celani, P.; Bernardi, F.; Robb, M. A. *J. Am. Chem. Soc.* **1998**, *120*, 2391−2407 and references therein.

(6) Morrison, H.; Lu, Y.-L.; Carlson, D. *J. Phys. Chem. A* **1998**, *102*, 5421−5432.

(7) Maciejewski, A.; Steer, R. P. *Chem. Rev.* **1993**, *93*, 67−98 and references therein.

(8) Turro, N. J.; Ramamurthy, V.; Cherry, W.; Farneth, W. *Chem. Rev.* **1978**, *78*, 125−145.

(9) Steer, R. P. *Rev. Chem. Intermed.* **1981**, *4*, 1 and references therein.

(10) Steer, R. P.; Ramamurthy, V. *Acc. Chem. Res.* **1988**, *21*, 380−386.

(11) McDonald, J. R.; Brus, L. E. *Chem. Phys. Lett.* **1972**, *16*, 587.

(12) Okabe, H. *J. Chem. Phys.* **1977**, *66*, 2058−2062.

(13) Szymanski, M.; Maciejewski, A.; Steer, R. P. *J. Phys. Chem.* **1992**, *96*, 7857−7863.

(14) Moule, D. C.; Burling, I. R.; Liu, H.; Lim, E. C. *J. Chem. Phys.* **1999**, *111*, 5027−5037.

(15) Moule, D. C.; Lim, E. C. *J. Chem. Phys.* **1999**, *110*, 9341−9344.

(16) Moule, D. C.; Judge, R. H.; Liu, H.; Lim, E. C. *J. Chem. Phys.* **2000**, *113*, 3937−3940.

(17) Moule, D. C.; Lim, E. C. *J. Phys. Chem. A* **2002**, *106*, 3072−3076.

(18) Fujiwara, T.; Moule, D. C.; Lim, E. C. *J. Phys. Chem. A* **2003**, *107*, 10223−10227.

(19) Clouthier, D. J.; Knight, A. R.; Steer, R. P.; Hackett, P. A. *Chem. Phys. Lett.* **1980**, *70*, 89−92.

(20) Levine, S. Z.; Knight, A. R.; Steer, R. P. *Chem. Phys. Lett.* **1974**, *29*, 73−76.

(21) Oka, T.; Knight, A. R.; Steer, R. P. *J. Chem. Phys.* **1975**, *63*, 2414−2420.

(22) Oka, T.; Knight, A. R.; Steer, R. P. *J. Chem. Phys.* **1977**, *66*, 699−706.

(23) Judge, R. H.; Moule, D. C. *J. Mol. Spectrosc.* **1980**, *80*, 363−373.

(24) Dixon, R. N.; Western, C. M. *J. Mol. Spectrosc.* **1986**, *115*, 74−81.

(25) Ludwiczak, M.; Latimer, D. R.; Steer, R. P. *J. Mol. Spectrosc.* **1991**, *147*, 414−430.

(26) Simard, B.; MacKenzie, V. J.; Hackett, P. A.; Steer, R. P. *Can. J. Chem.* **1994**, *72*, 745−754.

(27) Ondrey, G. S.; Bersohn, R. *J. Chem. Phys.* **1983**, *79*, 175−178.

(28) Einfeld, T. S.; Maul, C.; Gericke, K.-H. *J. Chem. Phys.* **2002**, *117*, 1123−1129.

(29) Warsylewicz, A. M.; Falk, K. J.; Steer, R. P. *Chem. Phys. Lett.* **2002**, *352*, 48−56.

(30) Fujiwara, T.; Lim, E. C.; Moule, D. C. *J. Chem. Phys.* **2003**, *119*, 7741−7748.

(31) Fujiwara, T.; Moule, D. C.; Lim, E. C. *Chem. Phys. Lett.* **2004**, *389*, 165−170.

(32) Kedzierski, W.; Borbely, J.; Mutus, J.; Amlin, S.; McConkey, J. W. *J. Chem. Phys.* **2004**, *120*, 9087−9089.

(33) Kapur, A.; Steer, R. P.; Mezey, P. G. *J. Chem. Phys.* **1979**, *70*, 745−748.

(34) Simard, B.; Bruno, A. E.; Mezey, P. G.; Steer, R. P. *Chem. Phys.* **1986**, *103*, 75−83.

(35) Strickler, B.; Gruebele, M. *Chem. Phys. Lett.* **2001**, *349*, 137−145.

(36) Frisch, M. J.; Trucks, G. W.; Schlegel, H. B.; Scuseria, G. E.; Robb, M. A.; Cheeseman, J. R.; Zakrzewski, V. G.; Montgomery, J. A.; Stratmann, R. E.; Burant, J. C.; Dapprich, S.; Millam, J. M.; Daniels, A. D.; Kudin, K. N.; Strain, M. C.; Farkas, O.; Tomasi, J.; Barone, V.; Cossi, M.; Cammi, R.; Mennucci, B.; Promelli, C.; Adamo, C.; Clifford, S.; Ochterski, J.; Petersson, G. A.; Ayala, P. Y.; Cui, Q.; Morokuma, K.; Malick, D. K.; Rabuck, A. D.; Raghavachari, K.; Foresman, J. B.; Cioslowski, J.; Ortiz, J. V.; Stefanov, B. B.; Liu, G.; Liashenko, A.; Piskorz, P.; Komaromi, I.; Gomperts, R.; Martin, R. L.; Fox, D. J.; Keith, T.; Al-Laham, M. A.; Peng, C. Y.; Nanayakkara, A.; Gonzalez, C.; Challacombe, M.; Gill, P. M. W.; Johnson, B. G.; Chen, W.; Wong, M. W.; Andres, J. L.; Head-Gordon, M.; Replogle, E. S.; Pople, J. A. *Gaussian 03*, revision A.1; Gaussian, Inc.: Pittsburgh, PA, 2003.

(37) MOLPRO is a package of ab initio programs written by Werner, H.-J. and Knowles, P. J., with contributions from Almlof, J.; Amos, R. D.; Cooper, D. L.; Deegan, M. J. O.; Dobbyn, A. J.; Eclert, E.; Elbert, S. T.; Hampel, C.; Lindh, R.; Lloyd, A. W.; Meyer, W.; Nicklass, A.; Peterson, K.; Pitzer, R.; Stone, A. J.; Taylor, P. R.; Mura, M. E.; Pulay, P.; Schutz, M.; Stoll, H.; Thorsteinsson, T.

(38) Helgaker, T.; Uggerud, E.; Jensen, H. J. A. *Chem. Phys. Lett.* **1990**, *173*, 145−150.

(39) Millam, J. M.; Bakken, V.; Chen, W.; Hase, W.; Schlegel, H. B. *J. Chem. Phys.* **1999**, *111*, 3800−3805.
(40) Hammond, G. S. *J. Am. Chem. Soc.* **1955**, *77*, 334−337.
(41) Lin, S. H. *J. Chem. Phys.* **1966**, *44*, 3759−3767.
(42) Turro, N. J. *Modern Molecular Photochemistry*; University Science Books: Herndon, VA, 1991.
(43) Harvey, J. N.; Aschi, M. *Phys. Chem. Chem. Phys.* **1999**, *1*, 5555−5563 and references therein.